Supplementary information

Creep and recovery analysis

In the 3-element model Kelvin-Zener model the measured strain ε is expressed as a function of the applied (constant) stress σ_0 and of the elastic constants (moduli) of the two elastic elements, G_1 and G_2 (second elastic element, part of the Kelvin-Voigt unit), and of the retardation time arising from the viscous element of the Kelvin-Voigt unit: $\varepsilon = \frac{\sigma_0}{G_1} + \frac{\sigma_0}{G_2}(1 - \exp(-t/\tau))$, or, expressed in terms of the compliance J, $J = \frac{1}{G_1} + \frac{1}{G_2}(1 - \exp(-t/\tau))$; this expression can be further rearranged in terms of the overall shear modulus G of the material and its instantaneous (glassy) compliance J_0:

$J = J_0 + \frac{1}{G}(1 - \exp(-t/\tau))$. 1/G in this case can also be termed retarded compliance J_r.

The above description, however, can be applied only in case of complete recovery, where the maximum recorded compliance of the material under stress is $J = J_g + \frac{1}{G}$ and, once the removed the stress, the compliance returns more or less rapidly to zero. In our experiments, this was a reasonable approximation only for the 70% Fmoc FF gel.

In case of incomplete recovery (plastic deformation = flow), as it is clearly the case for both 50% and 100% Fmoc FF gels, a viscous loss term cannot be avoided; in this case, the residual compliance value after recovery, which we can call J_{res}, is related to a steady state viscosity η of the materials: $\eta = \frac{t_{appl}}{J_{res}}$.

Graphically, this can be represented by the insertion of a dashpot in series to a Zener model (Figure 1 SI).

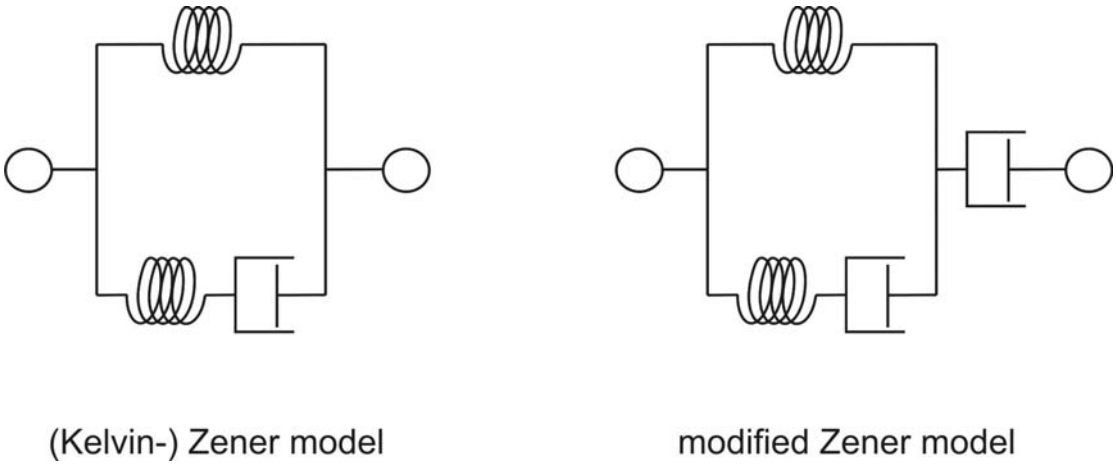

Figure 1 SI. Graphical representations of the Zener model (left) and of the modified Zener model utilized in this study

Using this modified model, the accord between experimental data and fits is excellent (Figure 2SI).

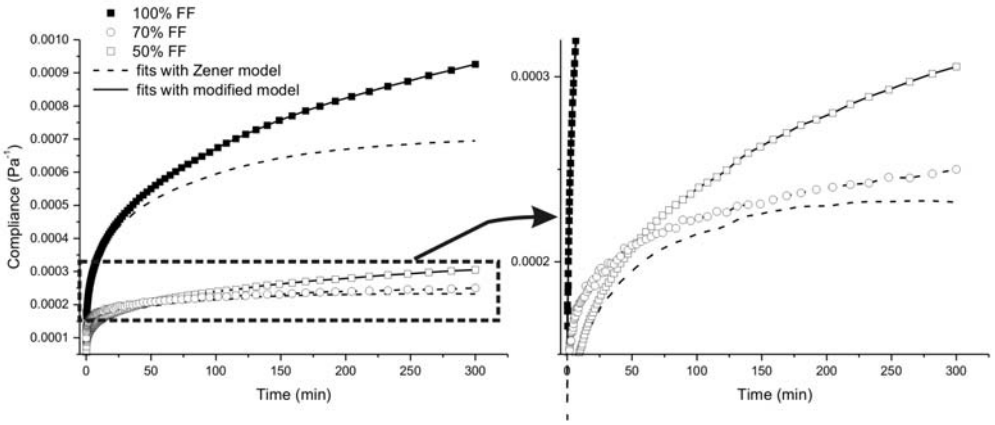

Figure 2 SI. Creep curves fitted with the Standard Linear Solid (Zener) model (dotted lines) and the modified Zener model (solid lines). The experimental data are plotted as black squares (100% FF), open circles (70% FF) and open squares (50% FF). Only for 70% FF the two models provide both valid fits, while for the other two systems the modified Zener models is clearly superior, since it takes into account the viscous flow.

NOTE: please realize that our approach is a significant approximation of a more realistic model where a distribution of relaxation (or retardation) times should be used; a function ofdistribution should therefore be introduced in the analytical expression of the compliance:

$$J = J_0 + \frac{1}{G}\int_0^{\infty} f(\tau)(1-\exp(-t/\tau))$$

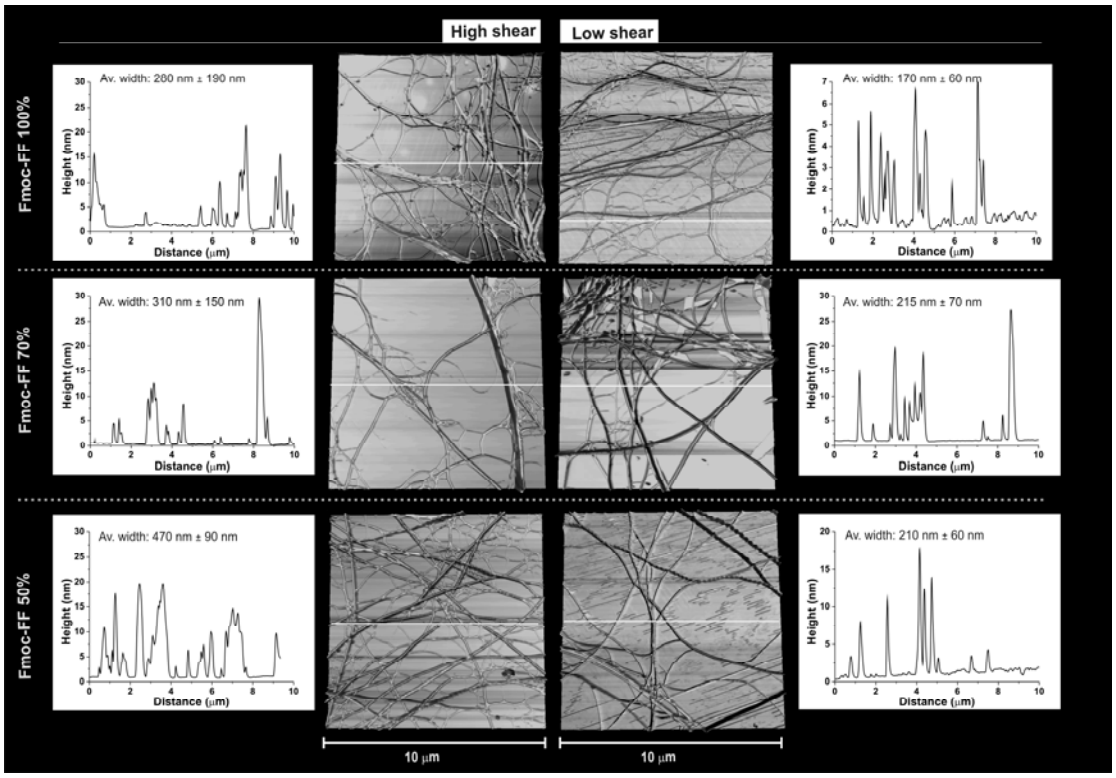

Figure 3 SI. 10*10 μm tapping mode AFM scans and representative height profiles (corresponding to the white bars in the AFM scans) for the different preparations investigated. The average width values were recorded on at least 60 different fibers

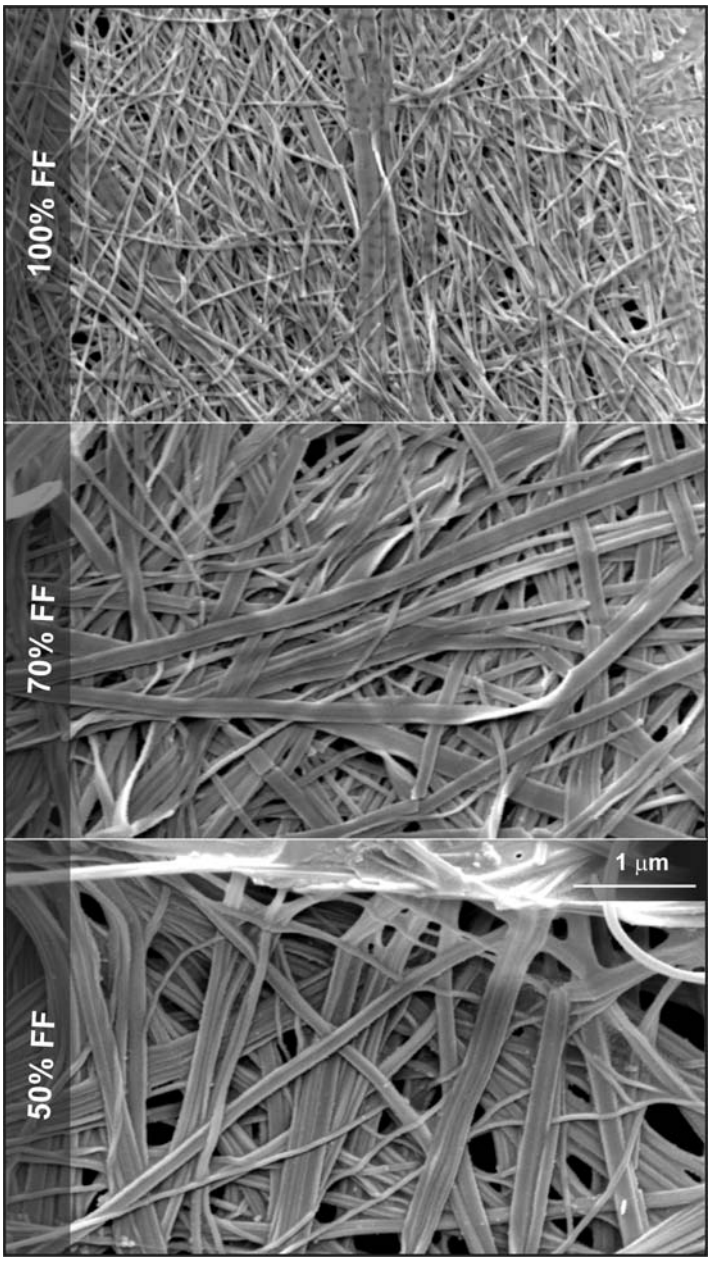

Figure 4 SI. CryoSEM images on “high shear” materials, showing a clear increase in lateral dimensions for the fibrillar aggregates (ribbons) with decreasing FF content.

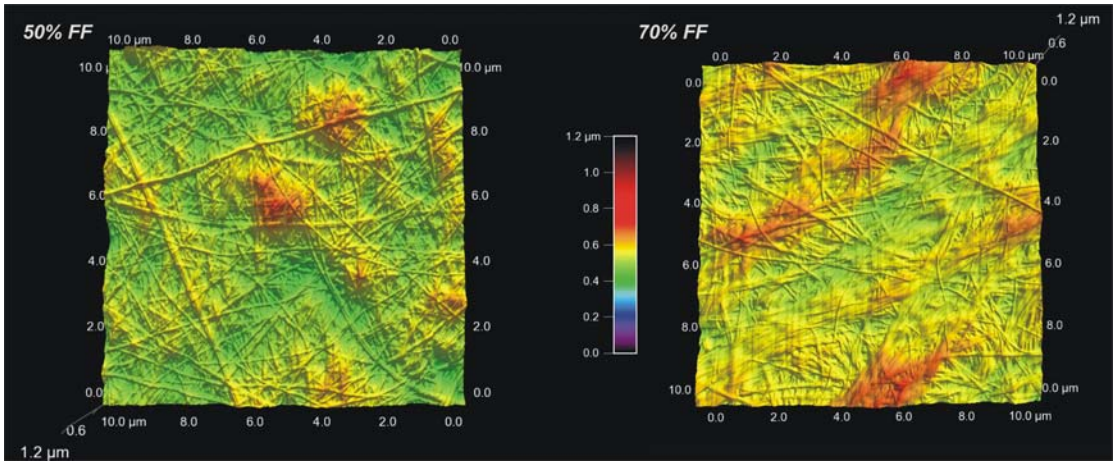

Figure 5 SI. Contact-mode scans of a 50:50 Fmoc-FF/GG (left) and a 70:30 Fmoc-FF/Fmoc-GG(right) "high shear" samples used for nanoindentation. These samples were obtained through the deposition of concentrated peptide dispersions (1% wt.). The different concentrations of the samples, however, did not seem to affect the morphology of the fibers; they appear substantially identical in lateral size and height to those obtained from the more dilute peptide dispersions used for imaging in tapping mode.